Giulio Maria Bianco, Abraham Mejia-Aguilar, and Gaetano Marrocco

Numerical and Experimental Characterization of LoRa-Based Helmet-to-Unmanned Aerial Vehicle Links on Flat Lands

A numerical-statistical approach to link modeling.

xxxxx

Use of the long-range (LoRa) communication protocol in a new generation of transceivers is attractive for search and rescue (SaR) procedures because they can operate in harsh environments, covering vast areas while maintaining low power consumption. The possibility of wearing helmets equipped with LoRa radios and installing LoRa transceivers in unmanned aerial vehicles (UAVs) will accelerate the localization of the targets, probably unconsciously. In this article, the achievable communication ranges of such links are theoretically and experimentally evaluated by considering possible positions of the helmet wearer (standing or lying) on a flat field, representing a simple SaR scenario. The simulations and experimental tests demonstrated that, for the standing position, the ground-bounce multipath produces strong fluctuations of the received power versus the transmitter-receiver (Tx-Rx) distances. Such fluctuations can be kept confined within 100 m from the target by lowering the UAV's altitude. Instead, for a more critical lying position, the received power profile is monotonic and nearly insensitive to the posture. For all the considered cases, the signal emitted by the body-worn transceiver can be exploited to localize the helmet wearer based on its strength, and it is theoretically detectable by the UAV radio up to 5 km on flat terrain.

Digital Object Identifier 10.1109/MAP.2022.3176590
Date of current version: 24 June 2022

INTRODUCTION

The aim of SaR operations is to localize a target person and then provide assistance. Such procedures are very common for both military and civilian purposes, particularly regarding the identification of first responders during fires,

earthquakes, and floods [1], [2] as well as in case of avalanches and to locate lost hikers [3]. Currently, ad hoc civilian SaR systems are used in mountain environments and rely on radio-frequency devices: avalanche beacons (also known as *ARVAs* [4]) and the RECCO system [5]. However, the effectiveness of those technologies is hampered by low ranges, which span from approximately 60 m (ARVA) to roughly 120 m at most (RECCO). Moreover, both devices cannot transmit any critical data about the user's health status. Improvements could come from Internet of Things (IoT) systems, exploiting recently developed low-power wide area networks (LPWANs) such as LoRa, Sigfox, and narrowband-IoT (NB-IoT) [6]. Thanks to their limited data rate, these networks can cover extended communication distances while maintaining very low power consumption [6]. They can thus enable connectivity even in the harshest environments.

LoRa is one of the most investigated LPWAN technologies as it was proven to reach a 30-km communication range by transmitting 25 mW [7]. Wearable LoRa devices are currently under study for several applications, ranging from tracking [8] to remote health monitoring [9]. The relevant use cases of LoRa are reported in Table 1. LoRa was also proposed for SaR applications where the communication range and power consumption are pivotal features. The authors recently proposed a LoRa-based IoT system for mountain SaR operations [14]. The system comprises body-worn LoRa radios and a range-based localization algorithm [21], exploiting received signal strength (RSS) measurements to localize the target when the GPS signal is absent. Thanks to the LoRa protocol's low energy consumption, the radios can support SaR operations for more than 5.5 h when they are fed with a typical battery of 1,100-mAh capacity [14]. Meanwhile, the target can be localized even with a small number of measurements collected quickly by employing classical range-based localization algorithms that exploit monotonic proportionality between the attenuation and Tx-Rx distance, as in [21]–[24]. However, only terrestrial LoRa links have been considered thus far, whereas in SaR scenarios, the terrestrial operations are complex and slow. Therefore, LoRa-based SaR could greatly benefit from UAVs searching the target from the sky. Indeed, by equipping a UAV with an LoRa Rx, many RSS measurements could be easily collected in a short time over a wide area.

Most first responders and hikers wear a safety helmet during operations and outdoor activities (like skiing or canyoneering), so the possible placement of an LoRa-wearable beacon is the helmet itself. Wearable helmet-mounted antennas were

SYMBOLS

The most relevant symbols used throughout the article are listed for the reader's convenience in order of appearance.

G_T	Radiation gain of the transmitting antenna
G_R	Radiation gain of the receiving antenna
ε	Electric permittivity: $\varepsilon_0[\varepsilon_r + j \cdot \mathrm{Im}(\varepsilon/\varepsilon_0)]$
ε_0	Permittivity of vacuum
σ	Electrical conductivity
P_R	Power collected by the receiving antenna
R	Unmanned aerial vehicle (UAV) radio helmet ground distance
H	Flying altitude of the UAV
h	Transmitter's height from ground
t	Terrain condition
P_T	Transmitting power
τ_T	Power transfer coefficient of the transmitting antenna
χ	Polarization loss factor
PL	Path loss
F	Path-gain factor
r	Ray path
d_0	Reference distance of the log-distance PL model
n	PL exponent
λ	Wavelength
Γ_T	Modulus of the reflection coefficient of the transmitting antenna
SF	Spreading factor
$\rho e^{j\psi}$	Fresnel reflection coefficient
θ_1'	Angle of departure of the reflected ray
θ_2'	Angle of departure of the direct ray
k_0	Propagation constant in the vacuum: $2\pi(\lambda)^{-1}$
φ	Grazing angle
$\hat{\rho}_T$	Polarization versor of the transmitting antenna
$\hat{\rho}_R$	Polarization versor of the receiving antenna.

TABLE 1. EXAMPLES OF RELEVANT USE CASES OF LoRa.

Reference	Topic	Reference	Topic
This work	Helmet-UAV off-body links for SaR	[13], [14]	Terrestrial links for mountain SaR
[8]	Localization and tracking	[15]	Emergency communications
[9]	Remote health monitoring	[16]	Extend SMS coverage to unconnected areas
[10]	Human activity recognition	[17]	Industrial monitoring
[11]	UAV communications for swarm configurations	[18]	Wireless underground sensor networks
[12]	Recovery of incapacitated UAVs	[19], [20]	Smart cities

proposed for disaster prevention [25] and military forces [26]. The more common helmet antennas are patches [26], dipoles [27], [28], and loops [29]. Noticeably, as stated in Table 1, a LoRa UAV-wearable device link [30] has never been neither characterized nor modeled. Moreover, all the helmet antennas proposed thus far are designed to work when the user is vigilant and standing so that effects of the ground when the wearer is unconscious or injured have not been addressed. Instead, if an accident happens, the user is likely lying on the ground, eventually in the presence of snow, and the helmet-UAV link is expected to be greatly affected by the helmet wearer's position.

This article aims at evaluating the performance of radio-helmet-to-UAV links when both standing and lying users are involved. Such off-body links [31], [32] are analyzed for the purpose of collecting, through a UAV, the LoRa RSS coming from a radio-helmet wearer and activating an SaR procedure (the latter is outside the scope of this article).

The modeling and experimentation are focused on line-of-sight (LoS) scenarios in flat lands. However, despite the simple approximation, the model can describe several SaR events, for example, 1) mountaineers in open environments hit by an avalanche, 2) lost hikers in some natural parks after fires, 3) injured soldiers in desert areas, and 4) missing citizens and first responders after cataclysms (such as earthquakes, tornadoes, and tsunamis) that destroy obstacles and create mostly flat and homogeneous zones. Within these conditions, the maximum LoRa communication ranges and the RSS stability versus the flight height and the UAV's distance are investigated here. The propagation model accounts for several positions of the helmet wearer (both standing and lying), the ground-bounce multipath, and the LoRa transmission parameters (namely, the variable sensitivity of the Rx). Furthermore, the basic model presented here can be extended to more complex environments by characterizing radio propagation of the considered site, either through measurement campaigns [14], [33], [34] or by ray-tracing simulations [35], [36].

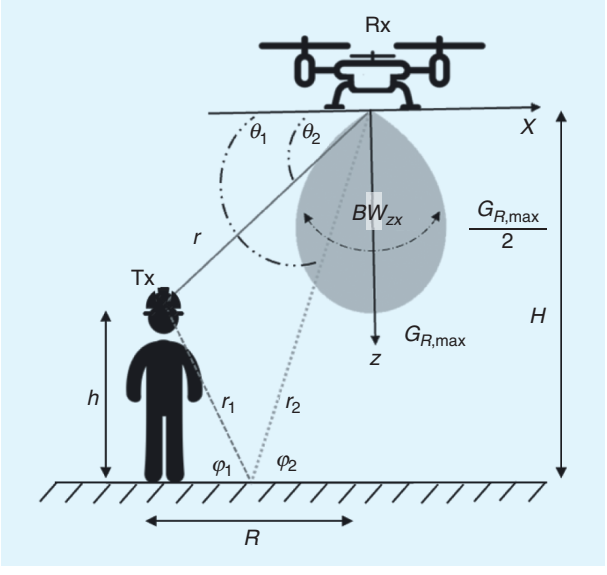

FIGURE 1. A sketch of the body-UAV link and relevant parameters.

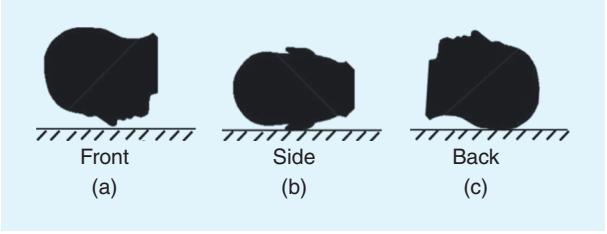

FIGURE 2. The three possible positions of a lying user on the (a) front, (b) side, and (c) back.

HELMET-TO-UAV LINK

With reference to Figure 1, the helmet-to-UAV link involves an LoRa transmitter (working in the 863–873-MHz LoRa band [37]) connected to a helmet antenna having radiation gain G_T and a UAV equipped with a receiving antenna of gain G_R. The user is assumed in four possible positions: standing, lying on the front, lying on the side, and lying on the back (Figure 2). Two reference boundary ground conditions are considered: a perfect electric conductor (PEC) ground (approximating a land covered by snow) and extremely dry terrain [i.e., rocks; permittivity $\varepsilon = \varepsilon_0(4.8 - 0.4j)$, electrical conductivity $\sigma = 10^{-4}$ S/m [38]]. The behavior of any real terrain is expected to include the aforementioned two extreme boundary conditions.

The helmet-to-UAV link is hence described by the power P_R collected by the Rx on the UAV according to the following link budget (all terms in decibel scale)

$$\begin{aligned} P_R(R,H,h,t) = {} & P_T + G_T(R,H,h,t) + G_R(R,H,h) \\ & + \tau_T(h,t) + \chi(R,H,h,t) \\ & - PL(R,H,h) + F(R,H,h,t), \end{aligned} \tag{1}$$

where P_T is the transmitting power, χ is the polarization loss factor, h is the Tx height from the ground, H is the flying altitude of the UAV, R is the UAV's ground distance from the target, and t is the terrain condition (dry or wet). The log-distance path-loss (PL) expression is $PL(r) = PL(d_0) + 10 \cdot n \cdot \log_{10}(r/d_0)$, with d_0 being a reference distance, n the PL exponent, and r the ray path. As LoS ground-to-air channels of low-altitude UAVs can be approximated by the free-space link [39], conditions $d_0 = \lambda/4\pi$ and $n = 2$ are assumed. Being Γ_T the modulus of the reflection coefficient of the transmitting antenna, $\tau_T = (1 - \Gamma_T^2)$ is the corresponding power transfer coefficient. The receiving antenna is instead considered perfectly matched to the Rx. The theoretical maximum communication distance is evaluated by imposing P_R equal to the Rx's sensitivity, which depends on the bandwidth and spreading factor (SF) of the LoRa signal, as listed in Table 2. Based on [14] and [41], a signal bandwidth of 125 kHz and a variable SF value are considered throughout the article. Finally, the term F is the path-gain factor that accounts for the multipath in the case of a standing user through the

flat-Earth two-ray propagation model [39], [42]. With reference to the geometrical parameters in Figure 1,

$$F = 20\log_{10}\left[\left|1+\rho e^{j\psi}\sqrt{\frac{G_T(\theta_1')G_R(\theta_1)}{G_T(\theta_2')G_R(\theta_2)}}\,e^{jk_0(r-r_1-r_2)}\right|\right], \quad (2)$$

where $|\cdot|$ is the absolute value operator, k_0 is the free-space propagation constant, $\rho e^{j\psi}$ is the Fresnel reflection coefficient, θ_2 identifies the direction of the direct path, and the antennas' gains are in linear scale. According to the Rayleigh criterion, the smooth terrain model still applies until the highest variation of the terrain's altitude, which can be approximated by a step, is less than $\lambda R[8(h+H)]^{-1}$; otherwise, the reflected field is weakened by diffuse scattering, and $|F|$ is reduced [43]. For instance, for $h = 1.7$ m and $H = 10$ m, a discontinuity of 0.5 m is negligible at 868 MHz when $R > 135$ m. The Fresnel reflection coefficient for an electromagnetic wave polarized parallelly to the ground is evaluated from the permittivity of the land itself as [42]

$$\rho e^{j\psi} = \frac{\sin\varphi - \sqrt{\frac{\varepsilon}{\varepsilon_0} - \cos^2\varphi}}{\sin\varphi + \sqrt{\frac{\varepsilon}{\varepsilon_0} - \cos^2\varphi}}. \quad (3)$$

For PEC-reflecting surfaces, then $\rho e^{j\psi} = -1$. If the user is lying, the antenna is on the ground, the multipath disappears, F is dropped out from (1), and the ground effect is accounted for in the gain of the helmet antenna, as described in the next section.

The link budget in (1) is parameterized here regarding the user's position (through the Rx gain) and the features of the receiving antenna.

MODEL OF THE Rx ANTENNA

The UAV is hereafter assumed to be equipped with a circularly polarized (CP) patch, as in [44]. The gain G_R (in linear scale) can be roughly approximated with an ellipsoid having rotational symmetry [45] whose elliptic section can be expressed in polar coordinates with respect to (w.r.t.) Figure 1

$$G_R(\theta) = \frac{2a_z^2 a_\xi \sin\theta}{a_z^2(\cos\theta)^2 + a_\xi^2(\sin\theta)^2}. \quad (4)$$

The patch is assumed to be the pole and lies on the (x, y) plane. The ellipse axes are hence

$$a_z = \frac{G_{R,\max}}{2} \quad (5)$$

$$a_\xi = a_z\cot\left(\frac{BW_{z\xi}}{2}\right), \quad (6)$$

where $\{G_{R,\max}, BW_{z\xi}\}$ are the maximum gain of the antenna and its half-power beamwidth, respectively.

MODEL OF THE Tx ANTENNA

The choice of reference helmet antenna could, in principle, consider both a linearly polarized or CP device for the Rx on board the UAV. A CP antenna would permit minimization of interference due to the ground as the reflection would invert the polarization verse so that the reflected field is filtered out by the Rx antenna having opposite polarization. However, using a CP antenna on the helmet too would introduce some drawbacks as polarization of the helmet antenna could be seen as reversed by the Rx because of the unpredictable Tx-Rx mutual positions during the UAV flight and the actual posture of the user. Sharp polarization mismatches could occur, thereby preventing establishment of communication. For the sake of generality, the transmitting antenna is assumed to be a flat dipole (a copper trace 35-μm thick) wrapped onto the top of the helmet (see Figure 3) according to two possible arrangements (w.r.t. the anatomical planes): along the median sagittal plane (hereafter referred to as the *sagittal dipole*), and the coronal plane (the coronal dipole). As shown in the "Polarization Loss Factor" section,

TABLE 2. SENSITIVITY OF THE LoRa SX1276 TRANSCEIVER FOR DIFFERENT *SF* VALUES AT A 125-KHZ BANDWIDTH [40].

SF	Sensitivity (dBm)
12	–136
11	–133
10	–132
9	–129
8	–126
7	–123

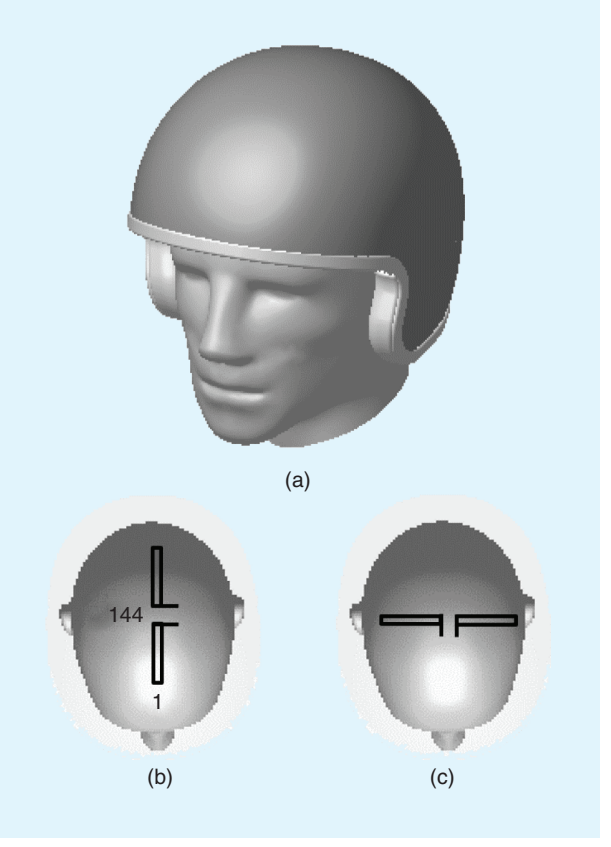

FIGURE 3. (a) Helmet and head numerical phantoms. The flat dipole (size in millimeters) along the (b) medial sagittal and (c) coronal planes.

this arrangement guarantees a reliable polarization matching in most conditions.

The gain G_T of the transmitting antenna is dependent on the working conditions. In particular, when the user is lying, interaction with the ground is expected to disturb the radiation pattern strongly. To simplify evaluation of the link budget in (1), the transmitting antenna is taken into account through an equivalent uniform gain pattern whose value is derived from statistical analyses involving the user's possible positions. For this purpose, radiation performances of all the combinations of antennas and positions are numerically evaluated utilizing the software CST Microwave Studio Suite 2018. The numerical model (available at https://grabcad.com/library/helmet-184) employed for the simulations includes

- the homogeneous numerical phantom of a human head with average relative permittivity and conductivity $\varepsilon_r = 42.7, \sigma = 0.99$ S/m [46], respectively
- a lossless foamed plastic ($\varepsilon_r = 1.5$ [47]) shell with the dimensions of a typical helmet for mountaineering (derived from the Vayu 2.0 model by Salewa, having a perimeter length of 63 cm)
- the ground modeled as a conducting plate.

The dipoles were preliminarily tuned at 868 MHz in the standing-user case so that the reflection coefficient is $\Gamma_T \leq -10$ dB in the whole LoRa band. Proximity with the PEC ground in the case of a lying user produces a moderate impedance mismatch (see Figure 4), nevertheless preserving the same maximum value as before. If the terrain is dry, reflection coefficients are less affected by the helmet's position and are more similar to the standing-user case.

By referring to the radiation gain patterns at the zenith (see Figure 5), it is clear that the two antenna layouts behave similarly for a standing user. In contrast, relevant differences are visible in the case of a lying user, with the maximum radiation

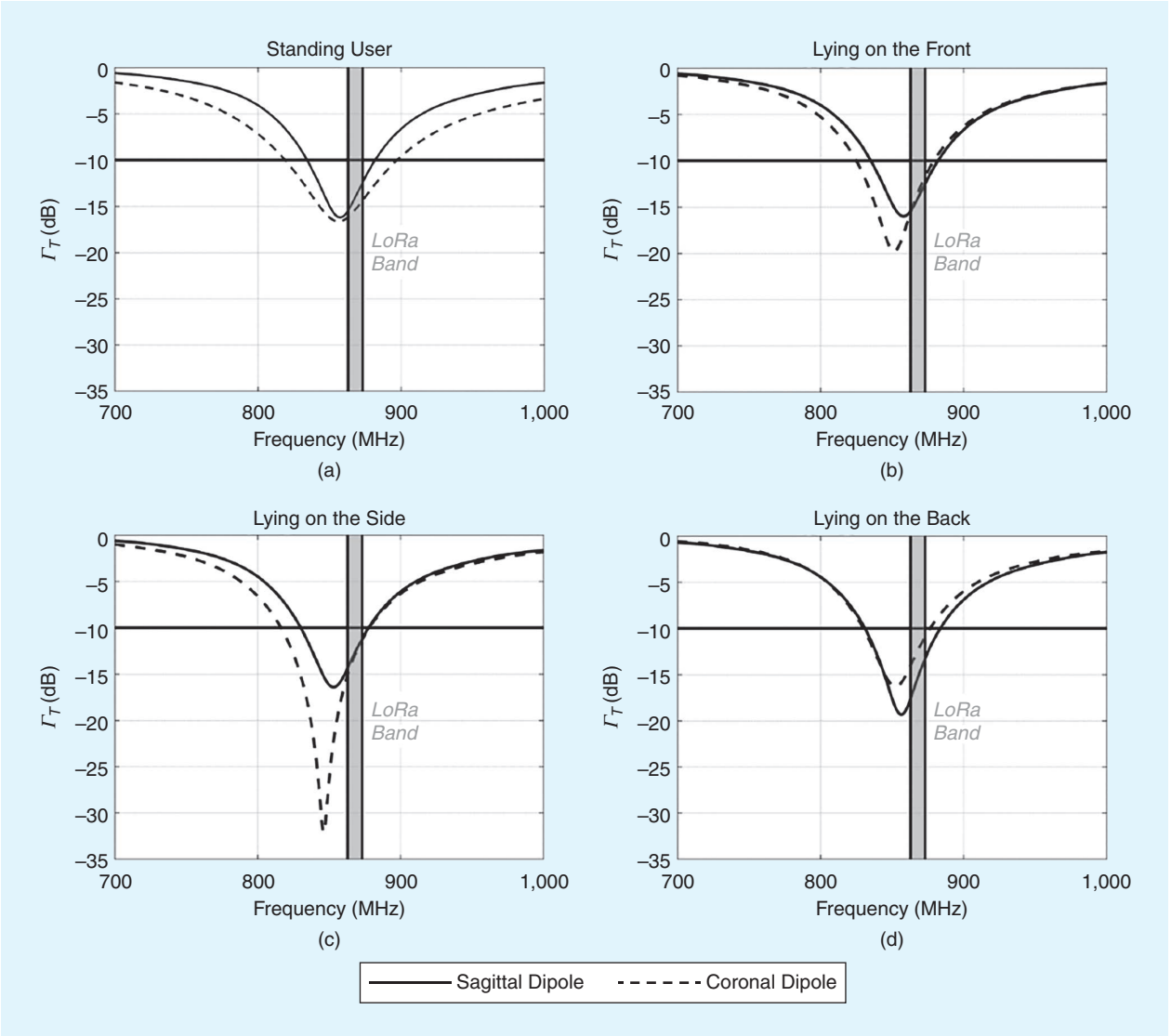

FIGURE 4. Simulated reflection coefficients of the helmet antennas in Figure 3 in four user positions over the PEC terrain. The LoRa 863–873-MHz band is highlighted in gray.

occurring either along the zenith or the horizon, depending on the position of the helmet.

The most appropriate antenna arrangement is the one maximizing the uniformity of the radiation pattern in the upper half space in all the considered user configurations, especially in the lying ones. The complementary cumulative distribution function (CCDF) for $G_T > G_0$ in the whole half space is used as a metric because CCDF(G_0) is the percentage of the half space where the gain of the antenna in all the three lying configurations is more than G_0, as shown in Figure 6(a). Accordingly, the coronal dipole outperforms the sagittal one. By considering, for instance, the threshold value of probability 75%, the corresponding lower bound gain $G_0(\text{CCDF} = 75\%)$ of the coronal dipole is approximately 2-dB higher than the corresponding value of the sagittal dipole.

In conclusion, the coronal dipole is hereafter considered the transmitting antenna whose equivalent gain is $G_T = G_0(\text{CCDF} = 75\%)$, keeping different values for standing and lying cases and kind of terrain, as summarized in Table 3.

POLARIZATION LOSS FACTOR

Like the antennas' gains, the polarization loss factor heavily varies with the helmet wearer's position and the terrain condition. The loss factor is evaluated from the polarization versors of the Tx ($\hat{\rho}_T$) and the Rx ($\hat{\rho}_R$) as

$$\chi = |\hat{\rho}_T \bullet \hat{\rho}_R^*|^2, \qquad (7)$$

with * and $\bullet$ being the complex conjugate and inner product operators, respectively.

To model polarization effects, polarization of the receiving CP patch is assumed constant and equal to $\hat{\rho}_R = \sqrt{2^{-1}}(1+j)$, whereas versor of the transmitting antenna is numerically evaluated when considering all the position-terrain combinations and all the possible observation angles [see Figure 6(b)]. From the simulations, $\chi \geq -3$ dB in 75% of the cases and, accordingly, the assumption $\chi = -3$ dB is considered for the next evaluation of the received power P_R.

LINK EVALUATION

Following the aforementioned framework, the radio-helmet-to-UAV link is numerically evaluated to predict the maximum achievable communication range and analyze the two-ray interference through coverage maps. The communication range is expressed as the radio-helmet-UAV ground distance as it is a

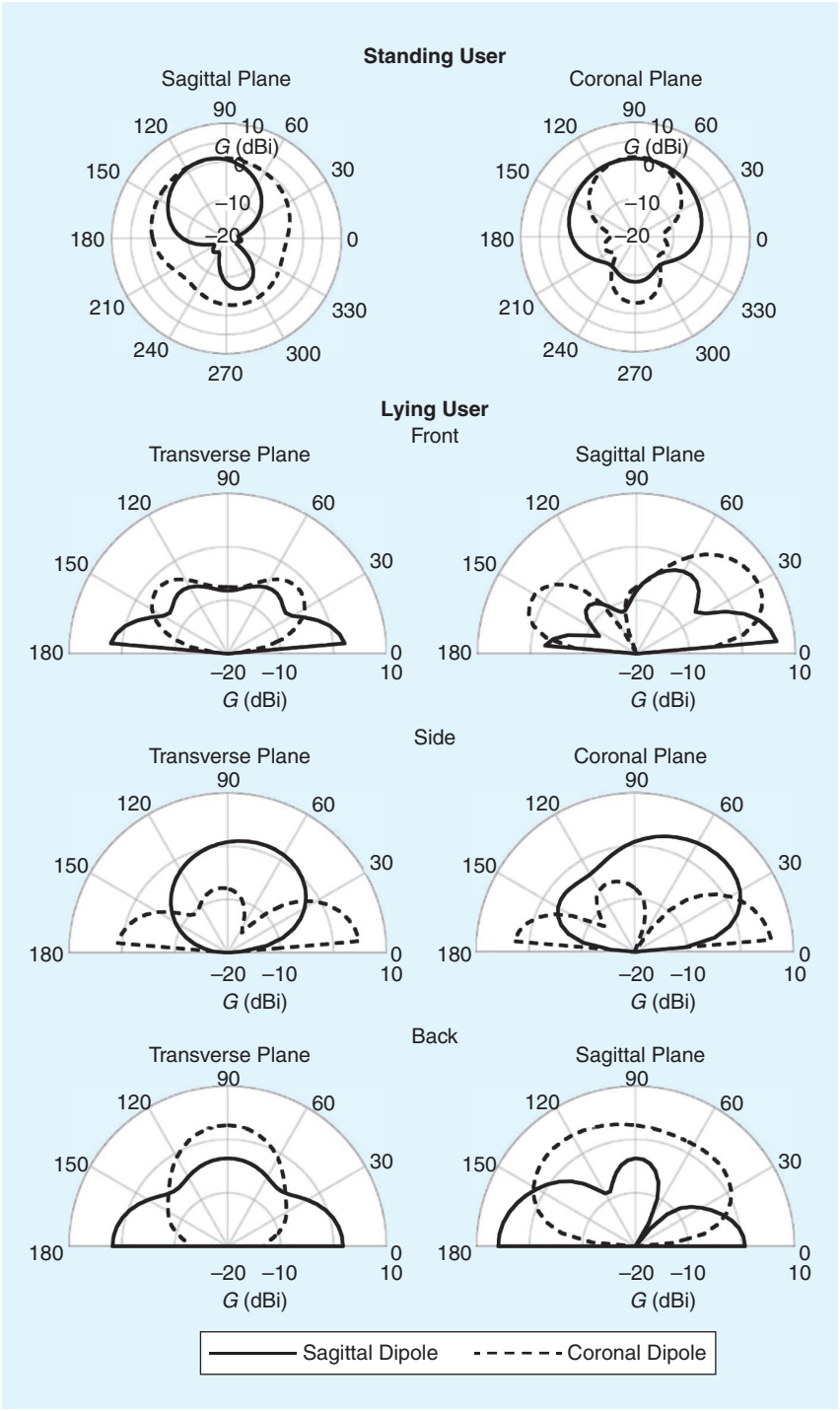

FIGURE 5. The simulated radiation gain of the helmet antennas (sagittal and coronal dipoles) over planes passing through the zenith. In the case of a lying user, a PEC ground is assumed. The dry terrain case returns the same patterns with an offset of −2 dB.

crucial parameter for most SaR operations. The user-UAV link must be as monotonic as possible to apply range-based location algorithms that exploit the RSS effectively.

The RSS is evaluated according to (1). The parameters of the receiving antenna to derive $G_R(\theta)$ are referred to as the *Keonn Advantenna-p11* ($BW_{z\xi} = 100°, G_{R,\max} = 3.2$ dBi), which is then used for the experimentation described in the next section. The received power at the UAV side is evaluated for a variable flight altitude $5\text{ m} \le H \le 120\text{ m}$ of the UAV, given that $H = 120$ m is the highest altitude of a UAV that is compliant with European Union (EU) regulations on civilian applications (open category) [48]. The corresponding maximum radio range $R_{\max}$, wherein the received power P_R equals the sensitivity of the Rx, is derived. Moreover, the Tx must comply with the effective radiated power (ERP) regulation for LoRa systems. By enforcing the EU's constraint [49] over the maximum LoRa irradiation (i.e., ERP=14 dBm at 868 MHz), the Tx is allowed to output $P_T = 14$ dBm. All computations refer to an $h = 1.7$-m-tall user. Finally, from Figure 4, $\tau_T(h,t) \simeq \tau_T = -0.01$ dB. The values of the parameters employed in the numerical simulations are resumed in Tables 3 and 4.

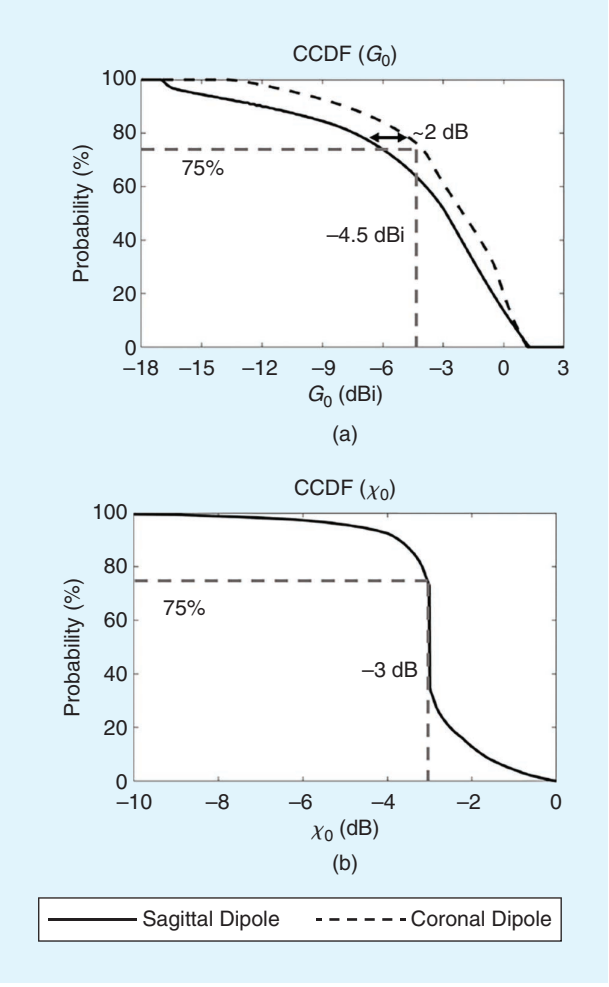

FIGURE 6. Complementary cumulative distribution functions. (a) CCDF (G_0) for the sagittal and coronal dipoles, taking into account the data of all three lying positions of the user on a PEC ground (see Figure 2) and (b) CCDF (χ_0) for the coronal dipole when considering both the standing and lying postures.

TABLE 3. THE SELECTED EQUIVALENT Tx GAIN G_0 (*CCDF* = 75%) FOR DIFFERENT USER AND TERRAIN CONDITIONS.

Standing User	–4.1 dBi	
Lying user	Wet terrain	Dry terrain
	–4.5 dBi	–6.5 dBi

Although both the lying and standing-user links are in LoS conditions, the evaluated RSS is rather different. First, by considering the standing-user case, Figure 7(a) shows the maximum estimated communication distances versus H for dry or wet terrains. The link range is mostly unaffected by the terrain's wetness, which instead impacts interference fringes, as shown next. The achievable $R_{\max}$ spans from approximately 3.8 to 6.5 km, depending on the *SF*. For instance, by increasing *SF* from 7 to 12, the predicted $R_{\max}$ for $H = 50$ m lengthens from 2 to 3 km. Focused coverage maps for $R \le 500$ m, wherein the interference pattern is highly variable, are depicted in Figure 7(b) and (c). The RSS is not monotonically related to the Tx-Rx distance, even in the ideal free-space case. The nulls in the RSS patterns are sharp due to the strong interference, especially for short, horizontal distances. Regarding the ground's condition, the wetter the terrain is, the stronger the reflected field is and, consequently, the more relevant the fluctuations are. An example of RSS profiles due to different terrain's wetness is shown in Figure 8. When comparing Figure 8(a) with Figure 8(b), it is evident that the fluctuations can be restricted to shorter distances R by lowering H. In particular, for $H = 15$ m, the interference fringes are restricted to R <100 m.

In the case of a lying user, the multipath is absent so that the RSS decreases monotonically with the Tx-Rx distance (see Figure 9). Unlike the previous case, the wetness of the terrain has a significant impact on the maximum range, especially for high-*SF* values. Indeed, if the wearer is lying on the ground, the on-helmet antenna's gain improves with a terrain wetness of 2 dB (as in Table 3), at most leading to a 21% higher radio range. The maximum communication range is up to 9.5 km if the terrain is wet, and hence, it is more extended than the corresponding distance in the case of a standing user.

TABLE 4. CONSIDERED VALUES FOR THE NUMERICAL RSS EVALUATION.

Parameter	Value	Parameter	Value
P_T	14 dBm	R	[0; 10,000] m
$G_{R,\max}$	3.2 dBi	H	[5; 120] m
$BW_{z\xi}$	100°	h (standing)	1.7 m
χ	–3 dB	h (lying)	0 m
f	868 MHz	τ_T	–0.01 dB

EXPERIMENTATION

The aforementioned numerical achievements are corroborated by preliminary experimentation with a UAV equipped with an LoRa Rx and a typical mountain helmet embedding a Tx to reproduce the simulated scenarios. Both vertical and horizontal flights are performed to verify the model's prediction.

The LoRa transmitting and receiving modules are Pycom LoPy-4 programmable boards (embedding the LoRa SX1276 transceiver; $P_T = 14$ dBm, bandwidth of 125 kHz, carrier frequency of 868 MHz, and coding rate of 4/5 [14]). The SF is set to SF = 12 to maximize Rx sensitivity and characterize the link as far as possible.

The transmitting antenna is a commercial dipole (by Pycom [50]) fixed on a Vayu 2.0 helmet for mountaineering along the coronal plane (see Figure 10). The helmet is worn by a 1.7-m-tall volunteer, as in the simulations.

The input parameter of the helmet-mounted dipole is measured by a portable Vector network analyzer (MS2024A by Anritsu) when the volunteer is standing and lying over dry and wet terrains. Overall, despite some frequency shifts between standing and fallen positions w.r.t. the nominal LoRa band, as predicted by the simulations (see Figure 4), the obtained reflection coefficient (see Figure 11) is always $\Gamma_T < 11$ dB at the useful frequencies, and it is well comparable with the simulated τ_T value presented in Table 4. The maximum observed downward frequency shift is roughly 55 MHz over all the conditions, so the helmet antenna must thus ensure a frequency bandwidth of at least 65 MHz to

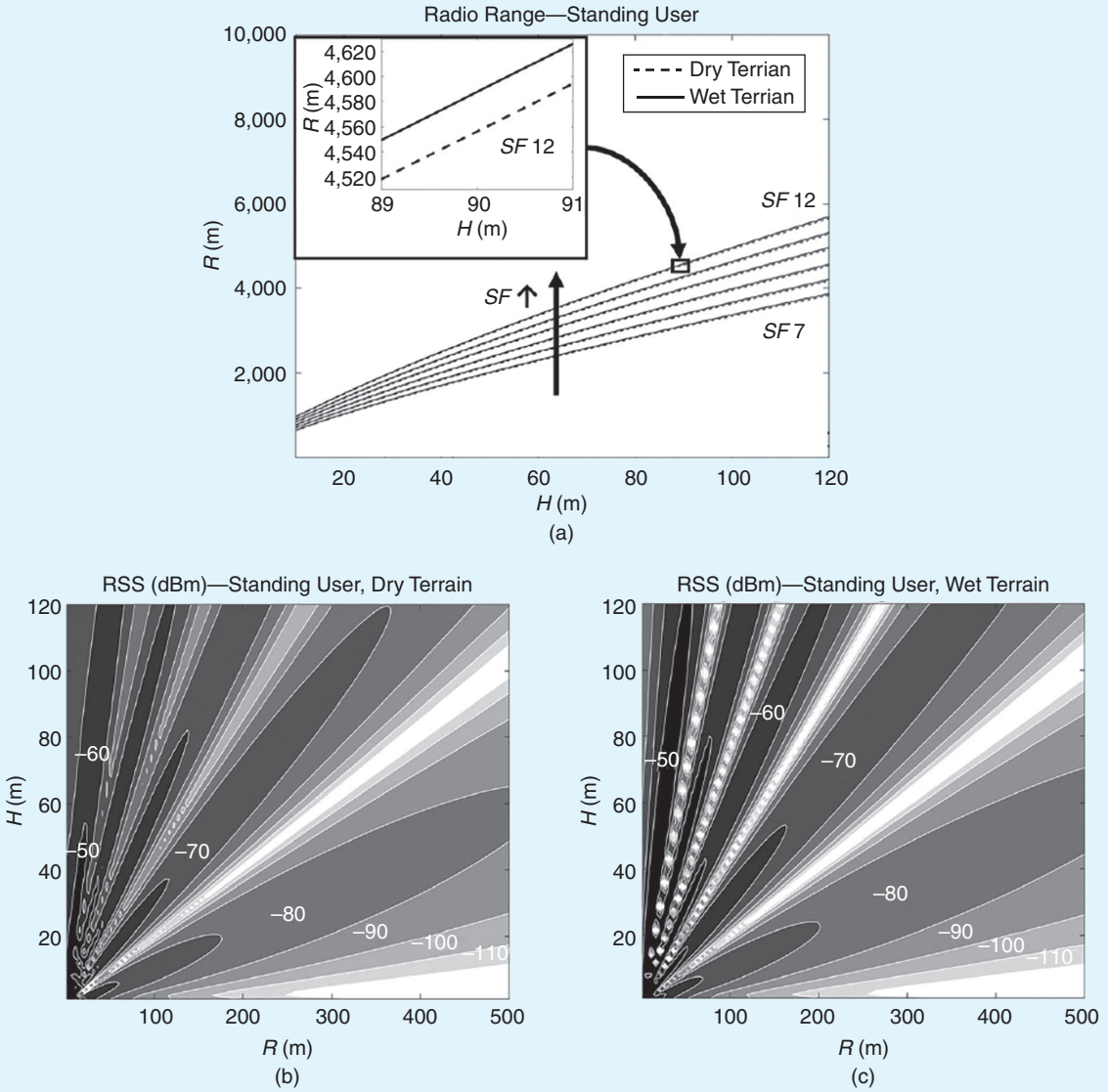

FIGURE 7. Theoretical coverage maps of the LoRa transmitting radio helmet and the UAV Rx in the standing-user case for different flying heights *H* and radial distances *R*. (a) Maximum communication distances versus the UAV height when varying the *SF* value in case of dry and wet terrains. The RSS for $R \leq 500$ m in case of a (b) dry terrain and (c) wet terrain.

cover the whole ultrahigh frequency LoRa band regardless of the wearer's posture.

The UAV is a DJI Phantom 3 Pro hosting a 137-mm × 137-mm CP patch (Keonn Advantenna-p11 as before). The battery pack and the LoRa Rx are fixed at the landing gear of the UAV, as illustrated in Figure 12.

The RSS measurements are performed during a period of consecutive sunny days over an uncultivated field near Colle Romito [Ardea, Lazio, Italy, GPS coordinates (41.551526, 12.567001); Figure 13(a)]. The field is flat [see Figure 13(b)] and covered by bushes. Thus, the test field can be considered dry ground. In the experiments, the UAV is driven at a 1-m/s approximate speed along both horizontal trajectories at fixed altitudes and vertical trajectories at a fixed radial distance from the user. The RSS in the dBm scale is estimated from the RSS indicator (RSSI) and from the SNR (signal-to-noise ratio) that are returned by the Rx [14]

$$P_R = \mathrm{RSSI} - 10\log_{10}\left(1+\frac{1}{\mathrm{SNR}}\right) + c_0, \tag{8}$$

where P_R is in dBm scale, the RSSI is in dB scale, the SNR is in linear scale, and c_0 (dBm scale) is a constant parameter obtained from a single-point calibration [40] through the Anritsu MS2711A spectrum analyzer.

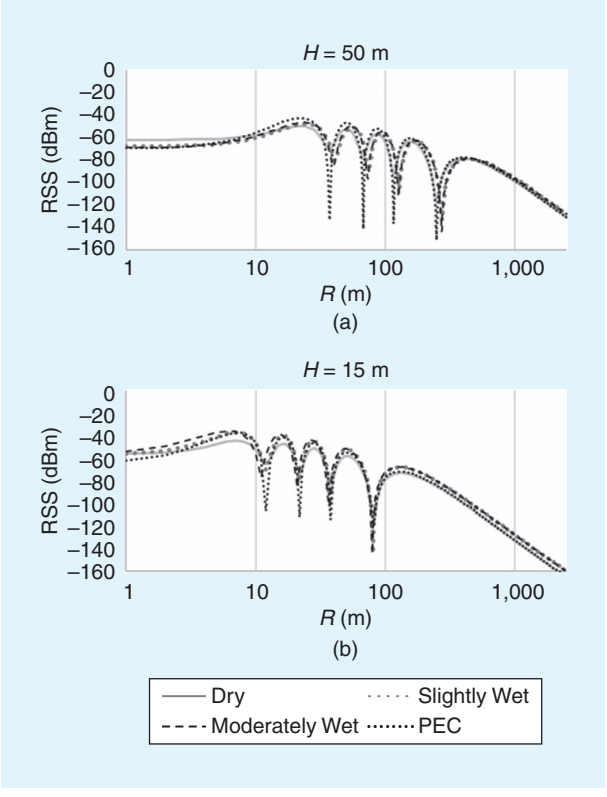

FIGURE 8. A numerically evaluated RSS for 1m $\leq R \leq$ 2,500 m and different terrain's wetness. The assumed intermediate permittivities are $\varepsilon_0(15-0.4j)$ for a slightly wet terrain and $\varepsilon_0(30-0.4j)$ for a moderately wet terrain [38]. Two different flying altitudes are considered: (a) $H = 50$ m and (b) $H = 15$ m.

In the first test, the UAV takes off at a distance of $R = 500$ m from the volunteer and then flies up vertically up to $H = 120$ m [see Figure 13(c)]. In the second test, the UAV flies horizontally at two fixed altitudes $H = \{50\text{ m}, 15\text{ m}\}$ for distances 1 m $\leq R \leq$ 2,700 m, as displayed in Figure 13(d). During the flights, 1,921 data packets are received overall.

The measured RSS profiles are reported in Figures 14 and 15 and compared with the simulated ones for vertical and horizontal flights, respectively. Interestingly, the RSS is rather insensitive to the lying user's particular position, and the modeling through a numerically evaluated equivalent gain is proven to be effective.

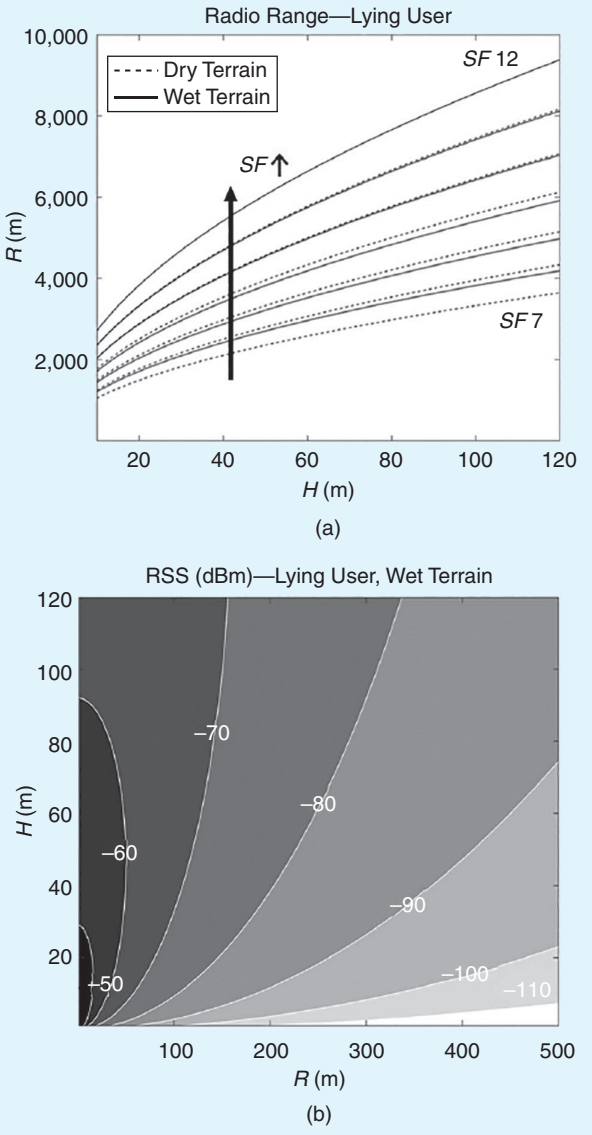

FIGURE 9. Theoretical coverage maps of the LoRa transmitting radio helmet and UAV Rx in the lying-user case. (a) The maximum communication distances versus UAV height when varying the *SF* value and (b) the RSS for $R \leq 500$ m (wet terrain).

Overall, in spite of some differences, the measurements corroborate phenomena derived by the numerical model in the "Link Evaluation" section (Figures 7 and 9), even in the presence of the significant multipath in the standing configuration. In detail, simulations overestimate the RSS of just 2 dB on the vertical and horizontal paths shown in Figure 14 and Figure 15(a), (b), and (d). Regarding Figure 15(c), there are some differences with the simulations at the end of the profile, where the model underestimates the RSS. The measured profile follows the flat-Earth two-ray model for $R \leq 700$ m, but afterward, it shows an intermediate behavior between the two- and single-ray propagation. In this condition, the combined effect of absorption by the low vegetation, scattering, and Earth elevation [see Figure 13(b)] attenuate the reflected field significantly [42]. The result is a weaker interference and, consequently, a lengthening of the link range, benefiting target identification from long distances.

The Tx-Rx distance also slightly affects the time delay between transmission and reception of the packets. In the performed flights, the measured delay ranges between 820 (at the shortest helmet-UAV mutual distance) up to 1,022 ms (upper-bound distance) and is comparable to the values reported in [51]. By considering the typical packet transmission rate (roughly one packet every 3 s), the aforementioned delays will not cause any loss of the received packet sequence. Accordingly, the observed packet-delivery ratio (PDR) in the experiments is of the order of 95% and nearly constant in all the cases. In more complex environments with non-flat grounds, the soft degradation of LoRa signals will lead to reduced radio ranges with the corresponding decrease of the PDR [7], [14]. Concerning the implications on localization, the time delay could slightly raise localization errors, especially if the target is moving. In SaR operations, however, the Tx is mostly stationary as the wearer could be fallen, or at most, slowly moving within a confined area. The corresponding error in estimating the position of the target is therefore expected to be modest. Furthermore, the UAV will generally get closer and closer to the target during SaR procedures so that the time delay reduces, the PDR increases, and the estimation of the target position is progressively refined.

It is worth specifying that, due to hardware constraints and law regulations, the aforementioned experimental tests did not allow us to appreciate the complete communication range corresponding to the last received packet. For this purpose, the UAV should have flown up to a much longer horizontal distance (R> 2,700 m), thus exiting from the test area and overflying various obstacles (houses, roads, and woods). Nevertheless, in past

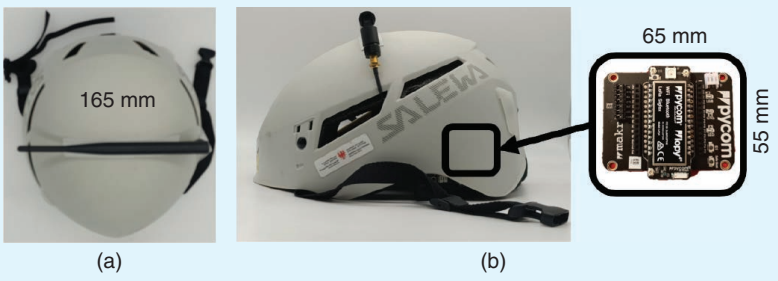

FIGURE 10. A radio-helmet prototype hosting a coronal dipole. (a) The top view and (b) side view with an indication of the LoPy-4 board installed in the interior of the helmet.

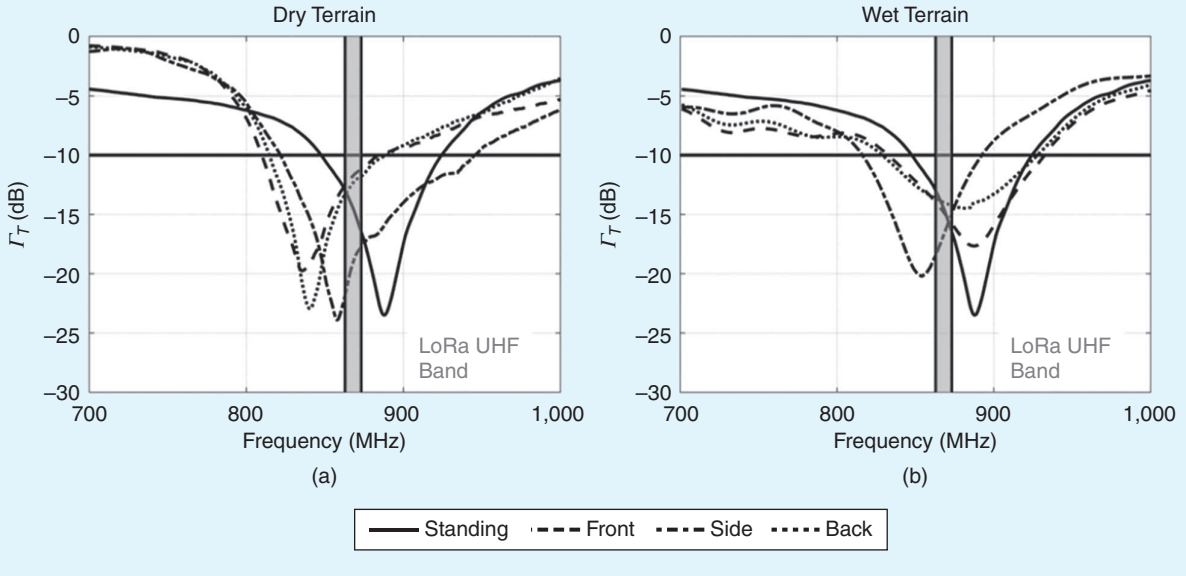

FIGURE 11. The measured reflection coefficient of the coronal dipole installed over the helmet when the wearer is standing and then lying on dry or wet terrain in the three postures.

experiments [13], we placed an LoRa radio over an 85-m-high overpass while the other radio was kept inside a car that was driven away from the overpass. This arrangement, comparable with the helmet-UAV system, achieved communications up to 8.4 km, in reasonable agreement with the numerical estimations.

DISCUSSION AND CONCLUSIONS

The helmet-to-UAV communication over flat lands based on the LoRa protocol has been numerically characterized and corroborated by a preliminary experimental campaign. The UAV is theoretically capable of collecting the helmet signal up to 5 km in a flat scenario even in the worst case (a standing user, perfectly flat, over wet terrain), and up to 9.5 km in case of wet terrain and a lying user when the UAV flies at an altitude of 120 m. The RSS in the case of a lying user is robust concerning the position of the helmet on the ground, and it monotonically decreases with the Tx-Rx distance. Instead, the RSS with a standing user (e.g., a lost hiker wandering on a snowy land) experiences fluctuations that are sharper the wetter the terrain, due to the ground-bounce multipath, especially near to the helmet's wearer.

FIGURE 12. A DJI Phantom 3 Pro UAV equipped with an LoRa Rx. The LoRa Rx is powered by a power bank and composed of a LoPy-4 board and Keonn Advantenna-p11 CP patch.

The basic model extension to a more complex radio propagation environment, including non-LoS links, can be quickly drawn if an equivalent log-distance PL model is available. For example, the authors recently modeled the LoRa propagation in snowy mountain fields, even when the Tx is buried [14]. Burying the Tx under 1 m of snow adds an entry loss of roughly 60 dB, which can be accounted for in the Tx's equivalent gain. Instead, the retrieved log-distance parameters for a Tx placed on the snow were $n = 3.17$ and $PL(d_0 = 1\,\text{m}) = 56.7$ dB, and these values are still approximately valid in the case of a lying user in a snowy plain. Hence, the PL model and the eventual path-gain factor must be inserted appropriately in the proposed link budget.

It is worth considering that the communication could be more challenging or even forbidden in harsher conditions that excessively reduce equivalent antenna gain, for instance, when the helmet is buried under more than 1 m of wet snow or deeply submerged by water (e.g., fallen into a river). In other cases, particular configurations of obstacles may highly raise the multipath and the shadowing, as we observed when the target was on the bottom of a canyon while the UAV was flying outside it [52].

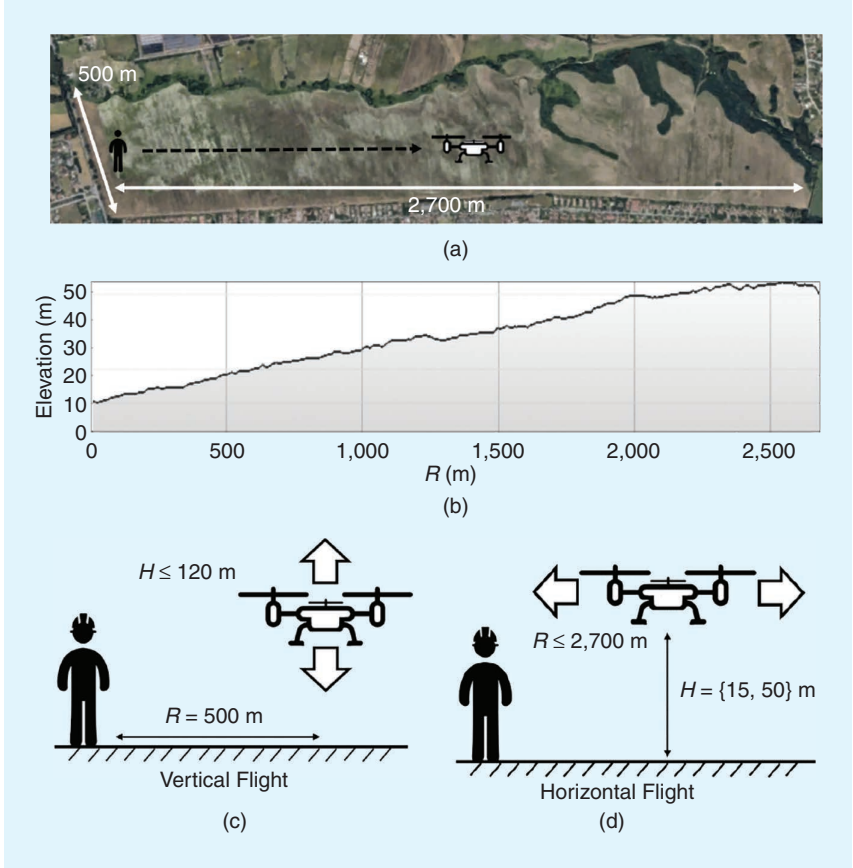

FIGURE 13. (a) A satellite view of the location for the experimental helmet-UAV LoRa link measurement, (b) an elevation profile of the field, (c) a sketch of the vertical flights, and (d) a sketch of the horizontal flights.

Finally, considering the model's application to SaR operations, the lying-user case is the most interesting because the user could be unconscious and even partially covered and, consequently, not detectable by a camera. The helmet wearer can be rescued through classic range-based localization algorithms like those mentioned in the "Introduction" section. Instead, in the case of a standing user, interference fringes make applying the aforementioned localization methods more challenging [53]. Spatial fluctuations can be mitigated by lowering the UAV's flying altitude. For instance, RSS oscillations are confined between 100 m, far from the target for an altitude of $H = 15$ m.

The fluctuations can also be reduced by placing the wearable antenna near the ground (e.g., on a boot). In any case, thanks to the local confinement of RSS fluctuations, the UAV can roughly estimate the target position from longer distances. Then, the UAV can approach the estimated location

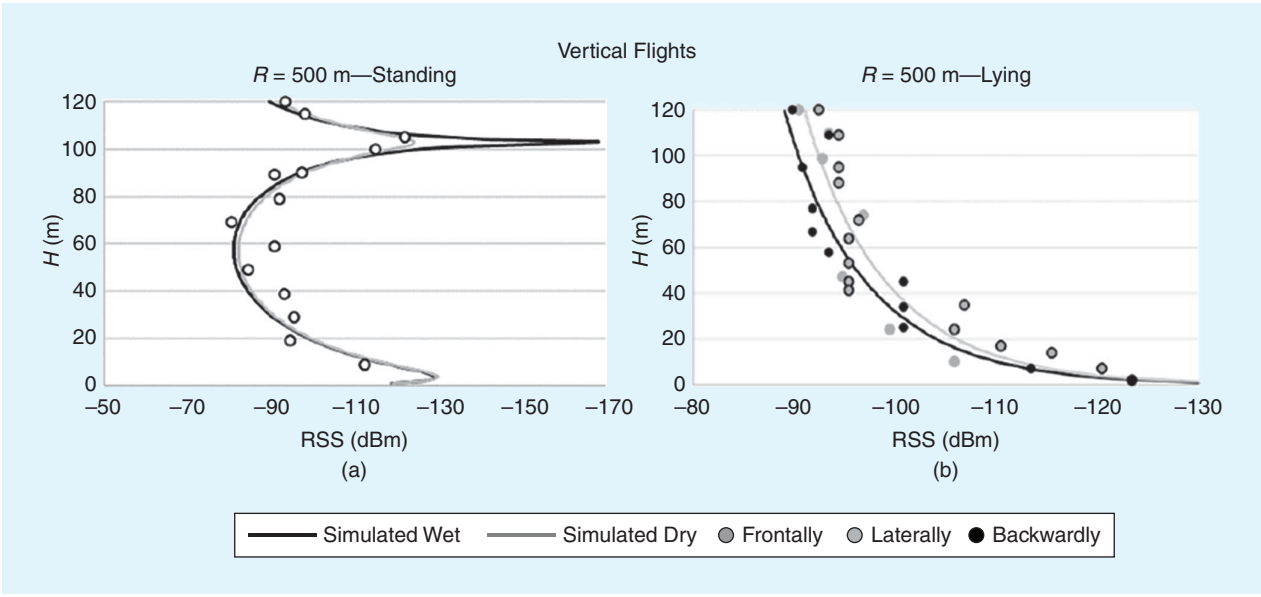

FIGURE 14. The RSS measured by the on-UAV LoRa ($SF = 12$) Rx during vertical flights at fixed ground distance $R = 500\ m$ from the Tx. The measurements for (a) a standing user and (b) a lying user.

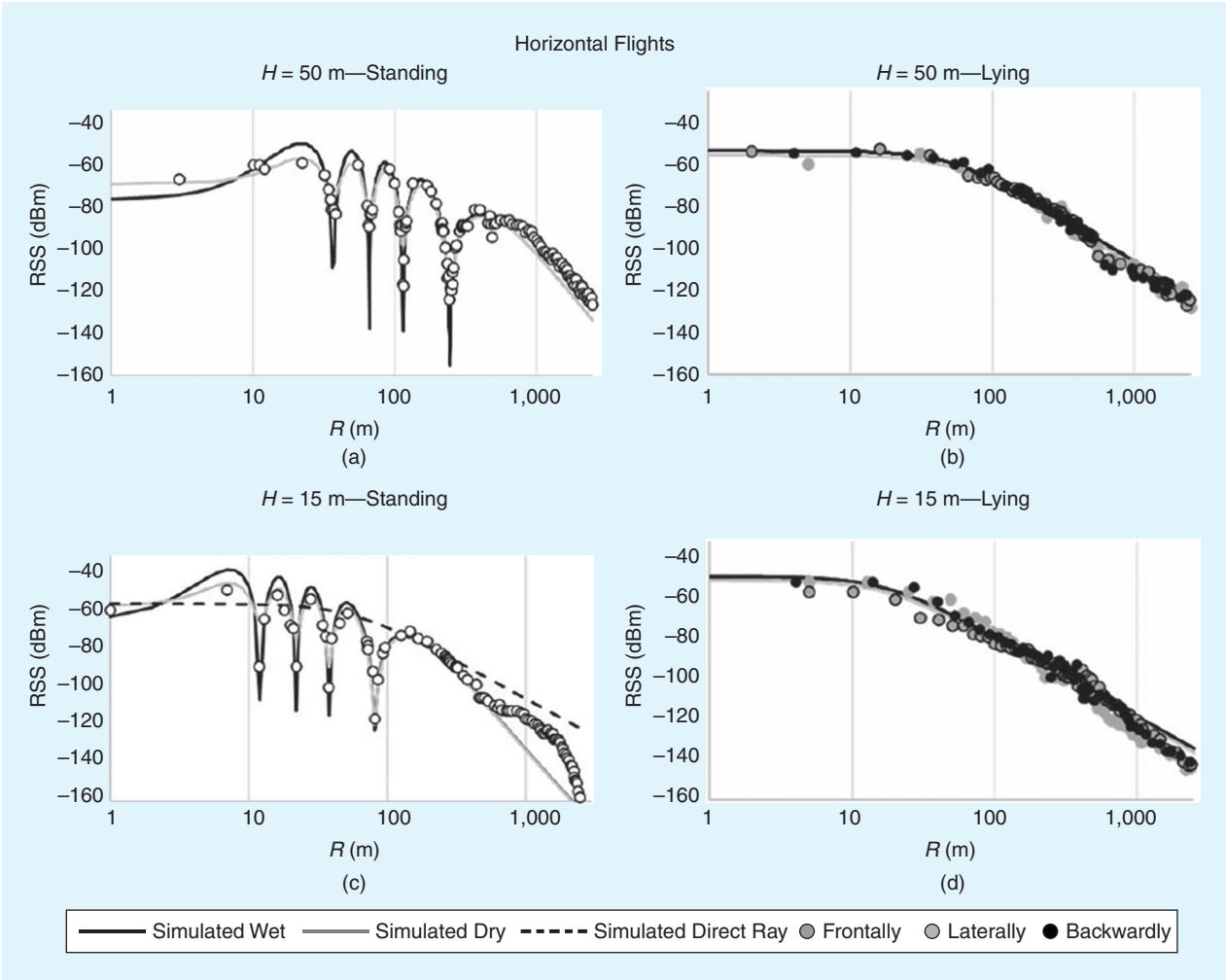

FIGURE 15. The RSS measured by the on-UAV LoRa ($SF = 12$) Rx during horizontal flights at different fixed flying heights H and for different user positions. (a) $H = 50$ m, standing user; (b) $H = 50$ m, lying user; (c) $H = 15$ m, standing user; and (d) $H = 15$ m, lying user.

and, when the signal begins fluctuating, it could use the support of optical or thermal cameras to reach the user, who is standing and, likely, conscious. Hence, while the high-RSS fringes are produced by the reflection from the flat ground when the user is standing, the eventual low-RSS fringes are generated by the multipath from nonflat terrains and will be observed for longer distances. Furthermore, the dynamic refinement of position estimation while approaching the target also allows for contrast of the packet's loss caused by the harsh environment. Regardless of the target's posture, the UAV could move along nonlinear trajectories to speed up the search, as proposed in [54] and [55], by dynamically accounting for signal variations and topology of the area. A swarm of multiple coordinated UAVs [56], [57] could also be deployed to provide data from different angles and distances to mitigate the multipath effect.

ACKNOWLEDGMENTS

This work is funded by the European Regional Development Fund (ERDF) under the Cooperation Programme Interreg V-A Italia Austria 2014–2020, ITAT3023, and Smart Test for Alpine Rescue Technology, and by the ERDF Operational Program Investment for Growth, jobs ERDF 2014–2020 under project number ERDF1094, and Data Platform and Sensing Technology for Environmental Sensing LAB-DPS4ESLAB. Giulio Maria Bianco is the corresponding author.

AUTHOR INFORMATION

Giulio Maria Bianco (giulio.maria.bianco@uniroma2.it) is a postdoctoral researcher with the Pervasive Electromagnetics Lab at the University of Rome "Tor Vergata" and RADIO-6ENSE srl, Rome, 00133, Italy, and is also with the Center for Sensing Solutions, Eurac Research, Bolzano, Italy. He received his Ph.D. degree in computer science, control, and geoinformation in collaboration with the European Academy of Bolzano. His research interests include the modeling of bodycentric wireless devices and communication. He is a Member of IEEE.

Abraham Mejia-Aguilar (abraham.mejia@eurac.edu) is a senior researcher at the Center for Sensing Solutions, Eurac Research, Bolzano, 39100, Italy. His current research interests include sensors and methods integration for in situ, proximal, and remote sensing scales. He is a Member of IEEE.

Gaetano Marrocco (gaetano.marrocco@uniroma2.it) is a full professor with the Pervasive Electromagnetics Lab at the University of Rome "Tor Vergata," Rome, 00133, Italy, where he also serves as director of the Medical Engineering School. His research interests include epidermal electronics and wireless sensing systems for biomedical engineering, aeronautics, and radio-frequency identification. He is a Senior Member of IEEE.

REFERENCES

[1] "Emergency support function #9: SEARCH AND RESCUE," N. H. Dept. of Fish and Game, Concord, NH, USA, Rep. ESF#9, 2006. Accessed: Feb. 12, 2021. [Online]. Available: https://prd.blogs.nh.gov/dos/hsem/wp-content/uploads/2015/03/ESF-9-Search-Rescue.pdf

[2] W.-T. Chiu *et al*., "A survey of international urban search-and-rescue teams following the Ji Ji earthquake," *Disasters*, vol. 26, no. 1, pp. 85–94, Dec. 2002, doi: 10.1111/1467-7717.00193.

[3] B. Soulé, B. Lefèvre, E. Boutroy, V. Reynier, F. Roux, and J. Corneloup, "Accidentology of mountain sports: Situation, review & diagnosis," Fondation Petzl, Crolles, France, 2014. [Online]. Available: https://www.researchgate.net/profile/Bastien-Soule/publication/271134898_Accidentology_of_mountain_sports_Situation_review_diagnosis/links/54be7d970cf2bc93c7a32bb2/Accidentology-of-mountain-sports-Situation-review-diagnosis.pdf

[4] "Avalanche Beacons operating at 457 kHz: Transmitter-receiver systems," European Telecommunications Standards Inst., Sophia Antipolis, France, ETSI EN 300 7181 V2.1.1, 2018. Accessed: Feb. 12, 2021. [Online]. Available: https://www.etsi.org/deliver/etsi_en/300700_300799/30071801/02.01.00_20/en_30071801v020100a.pdf

[5] *R9 Detector User Guide*, RECCO Company, Lidingö, Sweden, 2009. Accessed: Feb. 12, 2021. [Online]. Available: https://usermanual.wiki/RECCO/A-

[6] J. Bardyn, T. Melly, O. Seller, and N. Sornin, "IoT: The era of LPWAN is starting now," in *Proc. 42nd Eur. Solid-State Circuits Conf.*, Lausanne, France, 2016, pp. 25–30, doi: 10.1109/ESSCIRC.2016.7598235.

[7] J. Petäjäjärvi, K. Mikhaylov, A. Roivainen, T. Hänninen, and M. Pettissalo, "On the coverage of LPWANs: Range evaluation and channel attenuation model for LoRa technology," in *Proc. 14th Int. Conf. ITS Commun*., Copenhagen, Denmark, 2015, pp. 55–59, doi: 10.1109/ITST.2015.7377400.

[8] A. T. Nugraha, R. Wibowo, M. Suryanegara, and N. Hayati, "An IoT-LoRa system for tracking a patient with a mental disorder: Correlation between battery capacity and speed of movement," in *Proc. 7th Int. Conf. Comput. Commun. Eng.*, Kuala Lumpur, Malaysia, 2018, pp. 198–201, doi: 10.1109/ICCCE.2018.8539316.

[9] J. Petäjäjärvi, K. Mikhaylov, M. Hämäläinen, and J. Iinatti, "Evaluation of LoRa LPWAN technology for remote health and wellbeing monitoring," in *Proc. 10th Int. Symp. Med. Inf. Commun. Technol.*, Worcester, MA, USA, 2016, pp. 1–5, doi: 10.1109/ISMICT.2016.7498898.

[10] L. Shi, H. Xu, W. Ji, B. Zhang, X. Sun, and J. Li, "Real-time human activity recognition system based on capsule and LoRa," *IEEE Sensors J.*, vol. 21, no. 1, pp. 667–677, Jan. 2021, doi: 10.1109/JSEN.2020.3004411.

[11] Z. Yuan, J. Jin, L. Sun, K. Chin, and G. Muntean, "Ultra-reliable IoT communications with UAVs: A swarm use case," *IEEE Commun. Mag.*, vol. 56, no. 12, pp. 90–96, Dec. 2018, doi: 10.1109/MCOM.2018.1800161.

[12] P. A. Catherwood, M. Little, D. Finlay, and J. McLaughlin, "Recovery of incapacitated commercial delivery drones using LPWAN technology," *IEEE Intell. Transp. Syst. Mag.*, vol. 12, no. 2, pp. 6–19, Apr. 2020, doi: 10.1109/MITS.2019.2898972.

[13] G. M. Bianco, A. Mejia-Aguilar, and G. Marrocco, "Performance evaluation of LoRa LPWAN technology for mountain search and rescue," in *Proc. 5th Int. Conf. Smart Sustain. Technol.*, Split, Croatia, 2020, pp. 1–4, doi: 10.23919/SpliTech49282.2020.9243817.

[14] G. M. Bianco, R. Giuliano, G. Marrocco, F. Mazzenga, and A. Mejia-Aguilar, "LoRa system for search and rescue: Path-loss models and procedures in mountain scenarios," *IEEE Internet Things J.*, vol. 8, no. 3, pp. 1985–1999, Feb. 2021, doi: 10.1109/JIOT.2020.3017044.

[15] E. Sisinni, D. F. Carvalho, and P. Ferrari, "Emergency communication in IoT scenarios by means of a transparent LoRaWAN enhancement," *IEEE Internet Things J.*, vol. 7, no. 10, pp. 10,684–10,694, Oct. 2020, doi: 10.1109/JIOT.2020.3011262.

[16] F. Gimenez, C. Zerbini, and G. Riva, "Extending SMS service coverage in rural areas by using LoRa communication technology," (in Spanish), *IEEE Latin Amer. Trans.*, vol. 18, no. 2, pp. 214–222, Feb. 2020, doi: 10.1109/TLA.2020.9085273.

[17] H. P. Tran, W.-S. Jung, T. Yoon, D.-S. Yoo, and H. Oh, "A two-hop real-time LoRa protocol for industrial monitoring and control systems," *IEEE Access*, vol. 8, pp. 126,239–126,252, Jul. 2020, doi: 10.1109/ACCESS.2020.3007985.

[18] K. Lin and T. Hao, "Experimental link quality analysis for LoRa-based wireless underground sensor networks," *IEEE Internet Things J*, vol. 8, no. 8, pp. 6565–6577, Dec. 15, 2020, doi: 10.1109/JIOT.2020.3044647.

[19] M. S. Aslam *et al*., "Exploring multi-hop LoRa for green smart cities," *IEEE Netw.*, vol. 34, no. 2, pp. 225–231, Mar. 2020, doi: 10.1109/MNET.001.1900269.

[20] T. V. Pham *et al*.," "Proposed smart university model as a sustainable living lab for university digital transformation," in *Proc. 5th Int. Conf. Green Technol. Sustain. Develop.*, Ho Chi Minh City, Vietnam, Nov. 2020, pp. 472–479, doi: 10.1109/GTSD50082.2020.9303086.

[21] J. H. Lee and R. M. Buehrer, "Fundamentals of received signal strength-based position location," in *Handbook of Position Location: Theory, Practice, and Advances*, R. Zekavat and R. M. Buehrer, Eds. 1st ed. Hoboken, NJ, USA: Wiley, 2012, ch.11, pp. 359–395.

[22] G. M. Bianco, R. Giuliano, F. Mazzenga, and G. Marrocco, "Multi-slope path loss and position estimation with grid search and experimental results," *IEEE Trans. Signal Inf. Process. Netw.*, vol. 7, pp. 551–561, Aug. 2021, doi: 10.1109/TSIPN.2021.3106693.

[23] M. R. Gholami, R. M. Vaghefi, and E. G. Stram, "RSS-based sensor localization in the presence of unknown channel parameters," *IEEE Trans. Signal Process.*, vol. 61, no. 15, pp. 3752–3759, Aug. 2013, doi: 10.1109/TSP.2013.2260330.
[24] X. Li, "RSS-based location estimation with unknown pathloss model," *IEEE Trans. Wireless Commun.*, vol. 5, no. 12, pp. 3626–3633, Dec. 2006, doi: 10.1109/TWC.2006.256985.
[25] Y. Saita, T. Ito, N. Michishita, and H. Morishita, "Low-frequency inverted-F antenna on hemispherical ground plane," in *Proc. Int. Symp. Antennas Propag. Conf.*, Kaohsiung, Taiwan, 2014, pp. 183–184, doi: 10.1109/ISANP.2014.7026591.
[26] D. Kitching and F. Lalezari, "Low profile helmet mount GPS antenna," in *Proc. Conf. Tactical Commun.,* Fort Wayne, IN, USA, 1990, pp. 661–702, doi: 10.1109/TCC.1990.177764.
[27] N. Nishiyama, N. Michishita, and H. Morishita, "SAR reduction of helmet antenna composed of folded dipole with slit-loaded ring," in *Proc. Int. Symp. Antennas Propag.*, Hobart, Australia, 2015, pp. 1–2.
[28] N. Nishiyama, N. Michishita, and H. Morishita, "Low-frequency inverted-F antenna on annular ground plane," in *Proc. IEEE MTT-S Int. Microw. Workshop Series RF Wireless Technol. Biomed. Healthcare Appl.*, Taipei, Taiwan, 2015, pp. 143–144, doi: 10.1109/IMWS-BIO.2015.7303819.
[29] J.-Y. Park, H.-K. Ryu, and J.-M. Woo, "Helmet installed antenna using a half-wavelength circular loop antenna," in *Proc. IEEE Antennas Propag. Soc. Int. Symp.*, Honolulu, HI, USA, 2007, pp. 4176–4179, doi: 10.1109/APS.2007.4396461.
[30] A. Kachroo *et al.*, "Unmanned aerial vehicle-to-wearables (UAV2W) indoor radio propagation channel measurements and modeling," *IEEE Access*, vol. 7, pp. 73,741–73,750, May 2019, doi: 10.1109/ACCESS.2019.2920103.
[31] T. Ameloot, P. Van Torre, and H. Rogier, "LoRa base-station-to-body communication with SIMO front-to-back diversity," *IEEE Trans. Antennas Propag.*, vol. 69, no. 1, pp. 397–405, Jan. 2021, doi: 10.1109/TAP.2020.3008660.
[32] S. Dumanli, L. Sayer, E. Mellios, X. Fafoutis, and G. S. Hilton, "Off-body antenna wireless performance evaluation in a residential environment," *IEEE Trans. Antennas Propag.*, vol. 65, no. 11, pp. 6076–6084, Nov. 2017, doi: 10.1109/TAP.2017.2748362.
[33] T. O. Olasupo, "Wireless communication modeling for the deployment of tiny IoT devices in rocky and mountainous environments," *IEEE Sens. Lett.*, vol. 3, no. 7, pp. 1–4, Jul. 2019, doi: 10.1109/LSENS.2019.2918331.
[34] M. Simunek, F. P. Fontán, and P. Pechac, "The UAV low elevation propagation channel in urban areas: Statistical analysis and time-series generator," *IEEE Trans. Antennas Propag.*, vol. 61, no. 7, pp. 3850–3858, Jul. 2013, doi: 10.1109/TAP.2013.2256098.
[35] Z. Cui *et al.*, "Low-altitude UAV air-ground propagation channel measurement and analysis in a suburban environment at 3.9 GHz," *IET Microw., Antennas Propag.*, vol. 13, no. 9, pp. 1503–1508, Jul. 2019, doi: 10.1049/iet-map.2019.0067.
[36] N. E.-D. Safwat, F. Newagy, and I. M. Hafez, "Air-to-ground channel model for UAVs in dense urban environments," *IET Microw., Antennas Propag.*, vol. 14, no. 6, pp. 1016–1021, Apr. 2020, doi: 10.1049/iet-com.2019.0964.
[37] K. Mikhaylov, J. Petäjäjärvi, and T. Hänninen, "Analysis of capacity and scalability of the LoRa low power wide area network technology," in *Proc. 22nd Eur. Wireless Conf.*, Oulu, Finland, 2016, pp. 1–6.
[38] "Electrical characteristics of the surface of the Earth," International Telecommunication Union, Geneva, Switzerland, ITU-R P.527-4, 2017. Accessed: Feb. 12, 2021. [Online]. Available: https://www.itu.int/rec/R-REC-P.527-4-201706-I/en
[39] A. A. Khuwaja, Y. Chen, N. Zhao, M. Alouini, and P. Dobbins, "A survey of channel modeling for UAV communications," *IEEE Commun. Surveys Tuts.*, vol. 20, no. 4, pp. 2804–2821, 2018, doi: 10.1109/COMST.2018.2856587.
[40] "SX1272/73 Datasheet," Semtech Corp., Camarillo, CA, USA, 2017. Accessed: Feb. 12, 2021. [Online]. Available: https://www.mouser.com/datasheet/2/761/sx1272-1277619.pdf
[41] M. Bor and U. Roedig, "LoRa transmission parameter selection," in *Proc. 13th Int. Conf. Distrib. Comput. Sensor Syst.*, Ottawa, Canada, 2017, pp. 27–34, doi: 10.1109/DCOSS.2017.10.
[42] R. E. Collin, "Radio-wave propagation," in *Antennas and Radiowave Propagation*, New York, NY, USA: McGraw Hill, 1985, ch. 6, sec. 1, pp. 339–349.
[43] J. S. Seybold, "Fading and multipath Characterization," in *Introduction to RF Propagation*, Hoboken, NJ, USA: Wiley, 2005, ch. 8, sec. 2, pp. 166–186.
[44] G. Casati *et al.*, "The interrogation footprint of RFID-UAV: Electromagnetic modeling and experimentations," *IEEE J. Radio Freq. Identif. (2017–present)*, vol. 1, no. 2, pp. 155–162, Jun. 2017, doi: 10.1109/JRFID.2017.2765619.
[45] G. Marrocco, E. D. Giampaolo, and R. Aliberti, "Estimation of UHF RFID reading regions in real environments," *IEEE Antennas Propag. Mag.*, vol. 51, no. 6, pp. 44–57, Dec. 2009, doi: 10.1109/MAP.2009.5433096.
[46] IEEE Recommended Practice for Determining the Peak Spatial-Average Specific Absorption Rate (SAR) in the Human Head from Wireless Communications Devices: Measurement Techniques, IEEE 1528-2013, IEEE Standards Association, Piscataway, NJ, USA, Sep. 2013. [Online]. Available: https://standards.ieee.org/standard/1528-2013.html
[47] Y. H. Kim, S. W. Chan, J. Ahn, and S. H. Cho, "Studies of the variation in the dielectric constant and unique behaviors with changes in the foaming ratio of the microcellular foaming process," *Polym.-Plastics Technol. Eng.*, vol. 50, no. 8, pp. 762–767, Jun. 2011, doi: 10.1080/03602559.2010.551439.
[48] "Safe operation of drones in Europe," European Union Aviation Safety Agency, Cologne, Germany, Apr. 2018. Accessed: Nov. 5, 2020. [Online]. Available: https://www.easa.europa.eu/sites/default/files/dfu/217603_EASA_DRONES_LEAFLET%20%28002%29_final.pdf
[49] M. Saelens, J. Hoebeke, A. Shahid, and E. D. Poorter, "Impact of EU duty cycle and transmission power limitations for sub-GHz LPWAN SRDs: An overview and future challenges," *EURASIP J. Wireless Commun. Netw.*, vol. 2019, Sep. 2019, Art. no. 219, doi: 10.1186/s13638-019-1502-5.
[50] "LoRa (868MHz/915MHz) & Sigfox Antenna Kit," Pycom Company, Guildford, U.K., 2017. Accessed: Feb. 12, 2021. [Online]. Available: https://pycom.io/product/lora-868mhz-915mhz-sigfox-antenna-kit/
[51] E. D. Widianto, M. S. M. Pakpahan, A. A. Faizal, and R. Septiana, "LoRa QoS performance analysis on various spreading factor in Indonesia," in *Proc. Int. Symp. Electron. Smart Devices*, Bandung, Indonesia, Oct. 23–24, 2018, pp. 1–5.
[52] A. Mejia-Aguilar, G. M. Bianco, G. Marrocco, A. Voegele, M. van Veelen, and G. Strapazzon, "In-situ and proximal sensing techniques for monitoring natural hazards to mitigate risk in tourism activities: A case study in the Geoparc Bletterbach, Italy," in *Proc. IEEE Int. Geosci. Remote Sens. Symp.*, Brussels, Belgium, Jul. 11–16, 2021, pp. 1815–1818, doi: 10.1109/IGARSS47720.2021.9554279.
[53] R. J. R. Thompson, E. Cetin, and A. G. Dempster, "Unknown source localization using RSS in open areas in the presence of ground reflections," in *Proc. IEEE/ION Position, Location Navigation Symp.*, Myrtle Beach, SC, USA, Apr. 2012, pp. 1018–1027, doi: 10.1109/PLANS.2012.6236844.
[54] A. Buffi, A. Motroni, P. Nepa, B. Tellini, and R. Cioni, "A SAR-based measurement method for passive-tag positioning with a flying UHF-RFID reader," *IEEE Trans. Instrum. Meas.*, vol. 68, no. 3, pp. 845–853, Mar. 2019, doi: 10.1109/TIM.2018.2857045.
[55] S. A. A. Shahidian and H. Soltanizadeh, "Optimal trajectories for two UAVs in localization of multiple RF sources," *Trans. Inst. Meas. Control*, vol. 38, no. 8, pp. 908–916, Aug. 2016, doi: 10.1177/0142331214566026.
[56] H. Sallouha, M. M. Azari, A. Chiumento, and S. Pollin, "Aerial anchors positioning for reliable RSS-based outdoor localization in urban environments," *IEEE Wireless Commun. Lett.*, vol. 7, no. 3, pp. 376–379, Jun. 2018, doi: 10.1109/LWC.2017.2778723.
[57] Y.-J. Chen, D.-K. Chang, and C. Zhang, "Autonomous tracking using a swarm of UAVs: A constrained multi-agent reinforcement learning approach," *IEEE Trans. Veh. Technol.*, vol. 69, no. 11, pp. 13,702–13,717, Nov. 2020, doi: 10.1109/TVT.2020.3023733.